Regular Article

PHYSICAL CHEMISTRY RESEARCH
Published by the
Iranian Chemical Society
www.physchemres.org
info@physchemres.org

Phys. Chem. Res., Vol. 14, No. 1, 97-117, March 2026
DOI: 10.22036/pcr.2025.545064.2738

DFT Exploration, MEP, Molecular Docking, and Drug-Likeness as Potent Inhibitors of Monkeypox Viruses of Glucopyranoside Derivatives

Tasfia Tabassum and Sarkar M.A. Kawsar*

Laboratory of Carbohydrate and Nucleoside Chemistry (LCNC), Department of Chemistry, Faculty of Science, University of Chittagong, Chittagong-4331, Bangladesh

(Received 4 September 2025, Accepted 16 December 2025)

The synthesis and functionalization of carbohydrate derivatives play pivotal roles in advancing drug discovery and therapeutic development. Methyl-α-D-glucopyranoside (MGP) and its six derivatives have been selected for use as computational tools for drug discovery in medicinal chemistry. The structural and thermodynamic properties of the derivatives were optimized *via* density functional theory (DFT) with B3LYP/3-21G level theory. The subsequent analysis also examined the electronic energies, enthalpies, Gibbs free energies, heat capacity, entropy, HOMO–LUMO gaps, density of states, and molecular electrostatic potential (MEP) of these modified compounds. Molecular docking analysis was performed on these compounds with the targeted protein monkeypox virus (MPXV) to investigate their binding affinity and molecular interaction. Amino acid residues such as ARG127, ARG119, ASP10, ASP123, ASN78, THR120, HIS100, ARG129, ASN14, LYS16, GLU77, *etc*., have various binding affinities with ligands via hydrogen bonding and other nonbonding interactions. Although the parent compound successfully showed good findings, the derivatives of the compounds also presented improved pharmacokinetic properties, as shown by ADMET analysis. The collective findings from these studies suggest that MGP derivatives exhibit promising bioactive potential and could serve as effective targets for our proteins of interest.

Keywords: DFT, Methyl α-D-glucopyranoside, Molecular docking, Monkeypox virus, ADMET

INTRODUCTION

Carbohydrates represent a structurally diverse class of biomolecules that require multiple analytical techniques for comprehensive characterization [1]. These compounds are defined as the optically active polyhydroxy aldehydes or ketones that can be hydrolyzed to either of them [2]. Numerous distinct structures can be generated from simple monomeric units, combined with their tendency to exist as complex mixtures of closely related isomers, creating unique analytical challenges that surpass those encountered in protein analysis. Common analytical workflows include (i) isolation and purification of carbohydrate fractions, (ii) compositional analysis of monosaccharide constituents, (iii) controlled fragmentation of polysaccharides or glycosaminoglycans through partial hydrolysis or enzymatic cleavage [3], and (iv) separation and purification of the resulting oligosaccharide fragments, particularly when analyzing glycoconjugates that require the release of glycans from their protein or lipid anchors [4]. Carbohydrates are now considered highly relevant in disease mechanisms and therapeutic interventions because of their pivotal roles in biological recognition processes [5]. Different ring forms (pyranose, furanose), stereoisomers (α or β anomers), and substitution patterns can be adopted by carbohydrates, which leads to a vast array of structurally modified molecules [6]. This diversity covers enhanced binding affinity, solubility, and selectivity in drug design. Water solubility can increase because of the hydrophilic nature of carbohydrates, and their resemblance to naturally occurring sugars reduces the risk of severe toxicity. Compared with its free sugar counterpart, MGP is more stable, and it is a non-reducing sugar. Thus, it

*Corresponding author. E-mail: akawsarabe@yahoo.com

is a valuable scaffold in synthetic and medicinal chemistry [7]. Owing to its carbohydrate-protein interactions, it is considered a noble compound. Glucose structurally resembles MGP and is readily recognized by biological systems. This feature enables its participation in various biochemical, synthetic, and therapeutic processes. In recent years, methyl-α-D-glucopyranoside (MGP) with its derivatives has shown significant promising antimicrobial, anticancer, and enzyme inhibitory activities and has attracted interest as a building block for the synthesis of carbohydrate-based drugs. Numerous studies have shown that methyl α-D-glucopyranoside and its derivatives exhibit broad-spectrum bioactive properties, such as antifungal, antibacterial, anticancer, and antiviral activities, with particular relevance against various proteins [8]. These carbohydrate derivatives have been prioritized for computational evaluation of their interactions with various human pathogens, combining modern in silico techniques with traditional drug discovery approaches to assess their biological efficacy. Therapeutic progress based on the development of carbohydrates has progressed slowly because of many barriers, mainly for synthesis and analysis [9]. From 2000-2001, 54 carbohydrate-based drugs received approval for therapeutic or diagnostic application [10]. Numerous computational indicators, including molecular docking, ADME characteristics, the Lipinski rule, pharmacokinetics, drug likeness, and aquatic and nonaquatic toxicity, have been examined in several chains [11,12]. In addition to their structural and energetic roles, carbohydrates also perform essential regulatory functions across all domains of life. Protein activity can be modulated, and intercellular communication can be mediated in multicellular organisms, as proteins act as post-translational modifications. In plants, a wide range of biological activities are exhibited by low-molecular-weight glycosides with diverse glycosylation patterns. In the design of potent antiviral [13] and antimicrobial [14,15] agents, hydroxyl group modification of nucleoside and monosaccharide structures has been shown to be very successful. Carbohydrate-based cell walls function as dynamic barriers in microorganisms and provide protection while facilitating interactions with the surrounding environment.

Monkeypox is an enveloped double-stranded DNA virus that was first identified in humans in the Democratic Republic of the Congo in 1970 and is a zoonotic infectious disease caused by the monkeypox virus. This virus is a member of the Orthopoxvirus genus [16]. Initially, it was endemic to regions of Central and West Africa, but the virus gained international attention following outbreaks outside the continent, leading the World Health Organization to declare it a global public health emergency in 2022. This virus is clinically related to smallpox and presents similar symptoms, such as vesicular skin lesions, and historical smallpox vaccinations have been shown to provide a degree of cross-protection [17]. With thousands of confirmed cases across more than 100 countries, primarily in Europe and the Americas, the transcontinental reach was fully realized in the 2022 global outbreak. Including over 77,264 confirmed positive cases across 109 countries and territories, the event underscores the persistent threat of zoonotic diseases and their ability to cross geographical boundaries through modern trade and travel [18].

MPXV has a large, brick-shaped virion encased by a unique outer envelope, which is designed with specialized viral proteins that enable its initial attachment and entry into host cells. These surface proteins are prime targets for neutralizing antibodies. Currently, clinical trials for drugs that can work well against monkeypox are still investigating different methods, and clinical data on their efficacy against MPX are still emerging, with ongoing trials such as the STOMP study.Computational methods offer a powerful, cost-effective strategy, including molecular docking, simulations, and ADME/T predictions, to rapidly identify novel drug targets and evaluate potential ligands, thereby streamlining the therapeutic pipeline [19]. Notable medicinal potential was exhibited by most of the examined compounds predicted by the PASS and ADMET analyses, suggesting their suitability for future drug development. Docking analyses can be used in future investigations for the synthesis and experimental validation of the most promising derivatives. This research contributes to advancements in carbohydrate-based antiviral drug discovery and provides novel strategies for combating both current and emerging viral threats [20].

This study aims to integrate MGP derivatives as potential inhibitors against monkeypox virus (MPXV) via computational approaches. To accelerate the drug discovery process, *in silico* models have been successfully used. DFT

computations were used to investigate the geometric and electrical MGP and its derivatives. The physicochemical properties and pharmacokinetics of these compounds have also been investigated to determine the structural modifications and enhancements needed to act well against MPXV.

MATERIALS AND METHODS

Design and Optimization Method

MGP derivatives are designed by modifying the -OH groups or substituting the -CH_3 group with various acyl, alkyl, or aromatic moieties. ChemDraw was initially used to determine the 2D chemical structures of the parent compounds and their derivatives. These structures were then converted to 3D conformations [21]. The geometrical optimization was performed via computational software such as the Gaussian 09 program [22] and PyRx [23]. Density functional theory (DFT) at the B3LYP level with the 6-31G+(d,p) basis set was implemented in the Gaussian 09 W software package to predict the thermal and molecular orbital properties [24]. Properties such as the dipole moment, enthalpy, free energy, and frontier molecular orbital features, such as the HOMO and LUMO, were calculated from the optimized derivatives [25]. A proper design phase helps maintain the efficiency of structure-based optimization and molecular docking. Additionally, this helps to allow specific modifications of the parent molecule to improve its effects [26]. The designed synthetic derivatives were then combined with specific protein targets to assess their therapeutic potential.

Energy Minimization of Designed MGP Derivatives

To reduce the potential energy of a molecule and adjust its geometry according to the criteria, an energy minimization process is used (Fig. 1). This helps to obtain a more stable and realistic structure.

The raw structures may contain unrealistic bond angles, lengths, or steric clashes. To ensure accuracy, the stable conformations of the compounds were optimized. The 3D structure of the parent compound methyl α-D-glucopyranoside and its derivatives was put under a mathematical force field in computational software. After running the minimization, the position of the atoms of the compounds was adjusted accordingly. As a result, new optimized molecules serve as outputs with reduced energy, improved geometry, and no significant steric hindrance.

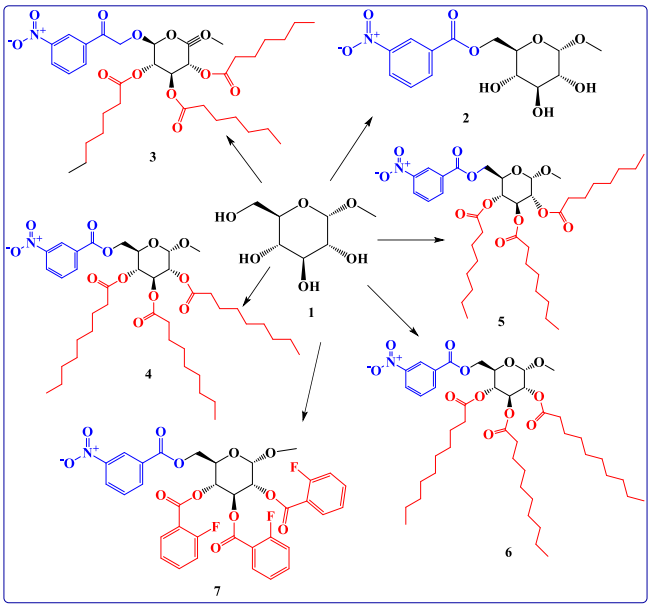

Fig. 1. 2D structures of methyl-α-D-glucopyranoside (entry **1**) and its derivatives (**2-7**).

Figure 2 shows the stable optimized structures of the MGP derivatives. This configuration clearly directs a point in the configuration space where forces acting on atoms are balanced altogether.

Protein Design and Molecular Docking

We obtained the three-dimensional structure of the monkeypox virus Zaire-96-I-16 (PDB: 4QWO) in PDB format from the Protein Data Bank [27,28]. To eliminate all heteroatoms and water molecules, PyMol (version 1.3) software programs were used [29]. For molecular docking, Swiss-Pdb reader software (version 4.1.0) was used to minimize protein energy consumption. After that, the best medications were subjected to molecular docking analysis against the protein that we were trying to target, Monkeypox Virus Zaire-96-I-16 (PDB: 4QWO). PyRx software (version 0.8) was used to produce a fine-grained molecular docking simulation, taking into account the drug as a ligand and the protein as a macromolecule.

Entry	Optimized structure	Entry	Optimized structure
1	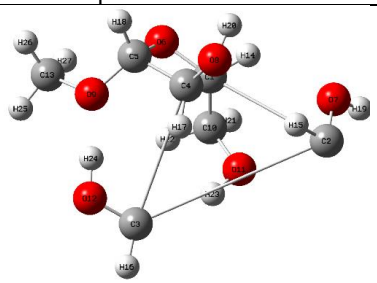	**2**	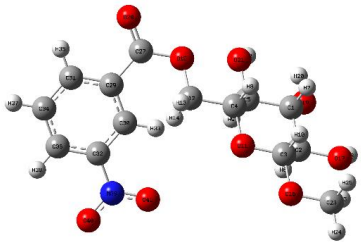
3	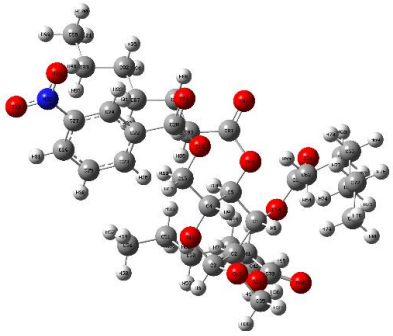	**4**	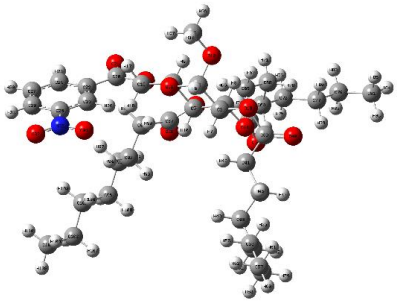
5	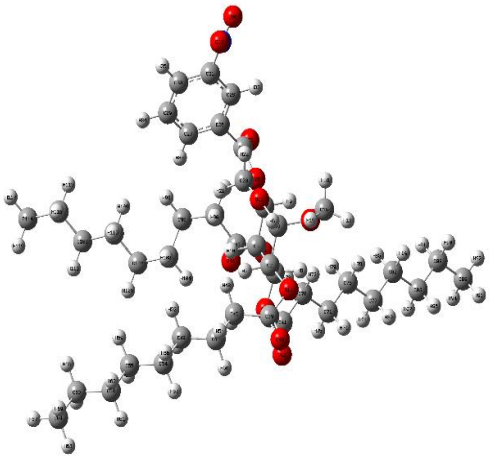	**6**	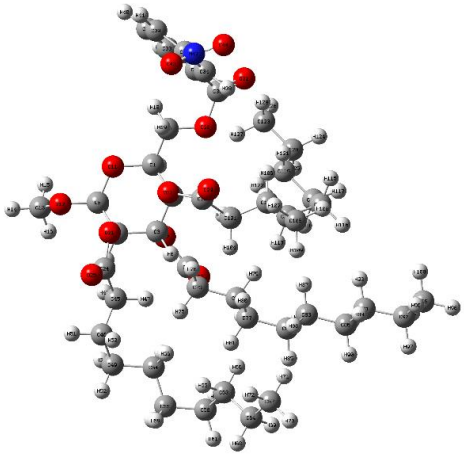
7	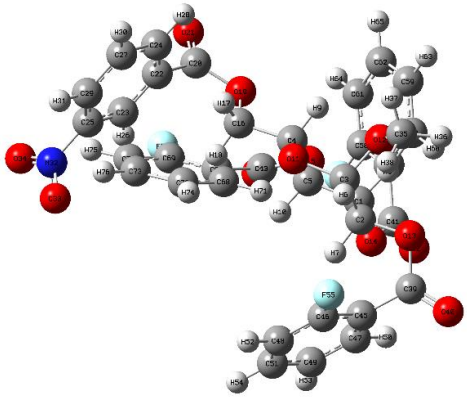		

Fig. 2. Optimized structures of 3D structures of MGP derivatives (entries **2-7**): Stable conformations found after DFT geometry optimization. These have the overall molecular geometry and the possible sites of ligand-protein interactions.

The MGL software package's AutoDock Tools (ADT) was utilized to transform pdb into a pdbqt format for input proteins and ligands, whereas AutodockVina was utilized for docking analysis. To analyze and visualize the docking outcomes and identify nonbonding interactions between ligands and receptor protein amino acid residues postdocking, the macromolecule and ligand structures were saved in pdbqt format, as mandated by Discovery Studio (version 4.1) [30]. Protein flexibility and mutual adaptability between receptors and ligands have now been acknowledged by the "hand-in-glove" concept, and this principle underpins two primary objectives: predicting the binding mode of small molecules to a protein target and estimating their (relative) binding affinities in structure-based computer-aided drug design (CADD) [31].

The docking results predict how ligand compounds fit into the binding site of a protein. Proper protein preparation leads to the addition of hydrogens, the removal of nonessential molecules, and the minimization of energy to relieve structural strain. Docking simulations may identify unreliable binding affinities if the protein is not correctly prepared, ultimately affecting drug design and further studies.

ADMET Study

ADMET analysis offers insights into critical factors such as solubility, permeability, bioavailability, plasma protein binding, metabolic stability, potential drug-drug interactions, and toxicity hazards. *In silico* ADMET uses computational simulations and modeling to predict a compound's behavior within an organism [32]. It serves as an alternative to *in vivo* testing. The 'drug-likeness' of a molecule is determined by the compound's 'drug-likeness' score. A greater 'drug-likeness' score of a chemical indicates superior quality. The analysis is typically performed *via* SWISSADME. The key physicochemical properties of approved drugs, such as molecular weight, hydrophobicity, and polarity, led to the creation of simple guidelines such as Lipinski's Rule of Five, Ghose's rule, QED, and RDL for drug discovery. To determine the property criteria required in an ideal compound, ADME properties with balancing toxicity have been analyzed. In early drug discovery, for the selection and design of compounds, toxic hazards must be balanced against other compounds [33]. Drug-likeness is typically assessed according to Lipinski's rule of five [34,35]. Poor solubility or rapid metabolism may require structural optimization of the drug, whereas severe toxicity signals might lead to the discarding of the compound. In recent years, ADMET has been an important aspect of drug development. It received the attention it truly deserves. A drug can be effective only when it is properly absorbed into the body. A drug must enter, circulate, persist for the required duration, and then be cleared for proper metabolism in the body [36].

RESULTS AND DISCUSSION

Frontier Molecular Orbital Analysis

Quantum mechanical approaches are crucial for determining the thermal, molecular orbital, and electrostatic characteristics of molecules in computational chemistry. Gaussian 09 software was used for geometry optimization and subsequent alterations of the generated derivatives. Frontier molecular orbitals are essential for analyzing chemical reactivity and kinetic stability, offering vital insights into a molecule's chemical stability and reactivity. The HOMO–LUMO gap influences chemical parameters such as softness, hardness, chemical potential, electronegativity, and electrophilicity [37,38]. Electronic absorption involves transitions from the ground state to the first excited state, predominantly by one-electron excitation from the highest occupied molecular orbital (HOMO) to the lowest unoccupied molecular orbital (LUMO). The molecular structures were visualized via GaussView 6.0.16 software. Comprehensive geometry optimization was conducted *via* density functional theory (DFT) at the B3LYP level *via* the 6-31G+(d,p) basis set, as implemented in the Gaussian 09 W software package. These computations yield insights into molecular stability and reactivity. The produced derivatives were examined via these quantum mechanical methods. The dipole moment, enthalpy, free energy, and entropy were computed for all the substances [39]. The values of chemical hardness, softness, and chemical potential are contingent upon the HOMO–LUMO energy. The kinetic stability increases as the HOMO–LUMO gap widens, resulting in a greater energy need for electron transfer from the ground HOMO state to the excited LUMO state [40]. The energies of the HOMO and LUMO, the HOMO–LUMO gap (Δ), the hardness (η), and the softness (S) of all the analogs are displayed in Table 1.

Table 1. Frontier Molecular Orbital Properties of the MGP Derivatives (**1-7**)

Entry	εHOMO (Hartree)	εLUMO (Hartree)	HOMO-LUMO gap (Hartree)	Hardness, ŋ	Softness, S
1	-0.47146	0.18174	0.6532	0.3266	3.061849357
2	-0.26285	-0.17773	0.08512	0.04256	23.4962406
3	-0.24455	-0.17468	0.06987	0.034935	28.62458852
4	-0.2431	-0.18155	0.06155	0.030775	32.49390739
5	-0.2439	-0.17606	0.06784	0.03392	29.48113208
6	-0.23837	-0.15879	0.07958	0.03979	25.1319427
7	-0.25206	-0.15762	0.09444	0.04722	21.17746717

For each derivative, the HOMO-LUMO energy gap, hardness (η), and softness (S) were computed *via* the energies of the frontier HOMO and LUMO in accordance with Parr and Pearson's interpretations of DFT and Koopmans' theorem via the following equation:

$$\text{Gap } (\Delta\mathcal{E}) = \varepsilon\text{LUMO} - \varepsilon\text{HOMO}$$

$$\eta = [\varepsilon\text{LUMO} - \varepsilon\text{HOMO}]/2$$

$$S = 1/\eta$$

In Table 1, the orbital energies of all the optimized compounds are represented by their softness and hardness. The hardness of these compounds gradually decreased, whereas their softness gradually improved with increasing number of chain lengths of the derivatives [40]. The highest softness was presented by compound **4 (**32.49390739), indicating that it has stronger chemical reactivity and polarizability than any other molecule. Therefore, compound 1 has the largest energy gap value (0.6532 Hartree). The highest hardness is given by compound **1** (0.3266**)**. The HOMO–LUMO gaps for the compounds can all be observed in Table 1. The energy gaps of these modified derivatives indicate their chemical reactivity, electronic properties, and stability. Compounds with lower gaps can easily donate or accept electrons, whereas a larger gap suggests greater stability [41]. The HOMO and LUMO iso-surfaces for methyl α-D-glucopyranoside and its derivatives (entries **1–7**) are displayed in Fig. 3, highlighting how the frontier electron density shifts with substitution. LUMO localization toward electron-withdrawing substituents and HOMO delocalization across the sugar ring vary, which illustrates the changes in potential reactive sites and charge-transfer pathways. The wavelength absorption and color of the compounds can be determined by the gap. This methodology is widely adopted in computational chemistry for reliable simulations. Overall, these techniques significantly enhance the understanding of molecular behavior and electronic transitions.

Thermodynamic Analysis

The free energy (G) and enthalpy (H) values are crucial for determining the reaction spontaneity and product stability, with more negative values indicating greater thermal stability [42]. In this study, all the modified MGP analogs presented more negative values for electronic energy (E), enthalpy (H), and free energy (G) than did the parent MGP. Table 2 shows the thermodynamic properties of the parent compound and its synthesized derivatives. The molecular weight increased from compound **1** (194.18 g mol^{-1}) to compound **6** (806.03 g mol^{-1}), indicating increasing structural features and chemical modifications. Compound **6** was observed to have the most negative Gibbs free energy, indicating that it has the highest thermodynamic stability among all the compounds. The chemical potential (μ) determines the reactivity and stability of molecules in a system. A more negative chemical potential indicates a greater and stronger tendency to undergo spontaneous reactions [43]. In this study, the MGP analogs presented lower (more negative) chemical potentials than did the parent compound and ranged from -0.20484 to -0.14486 Hartrees.

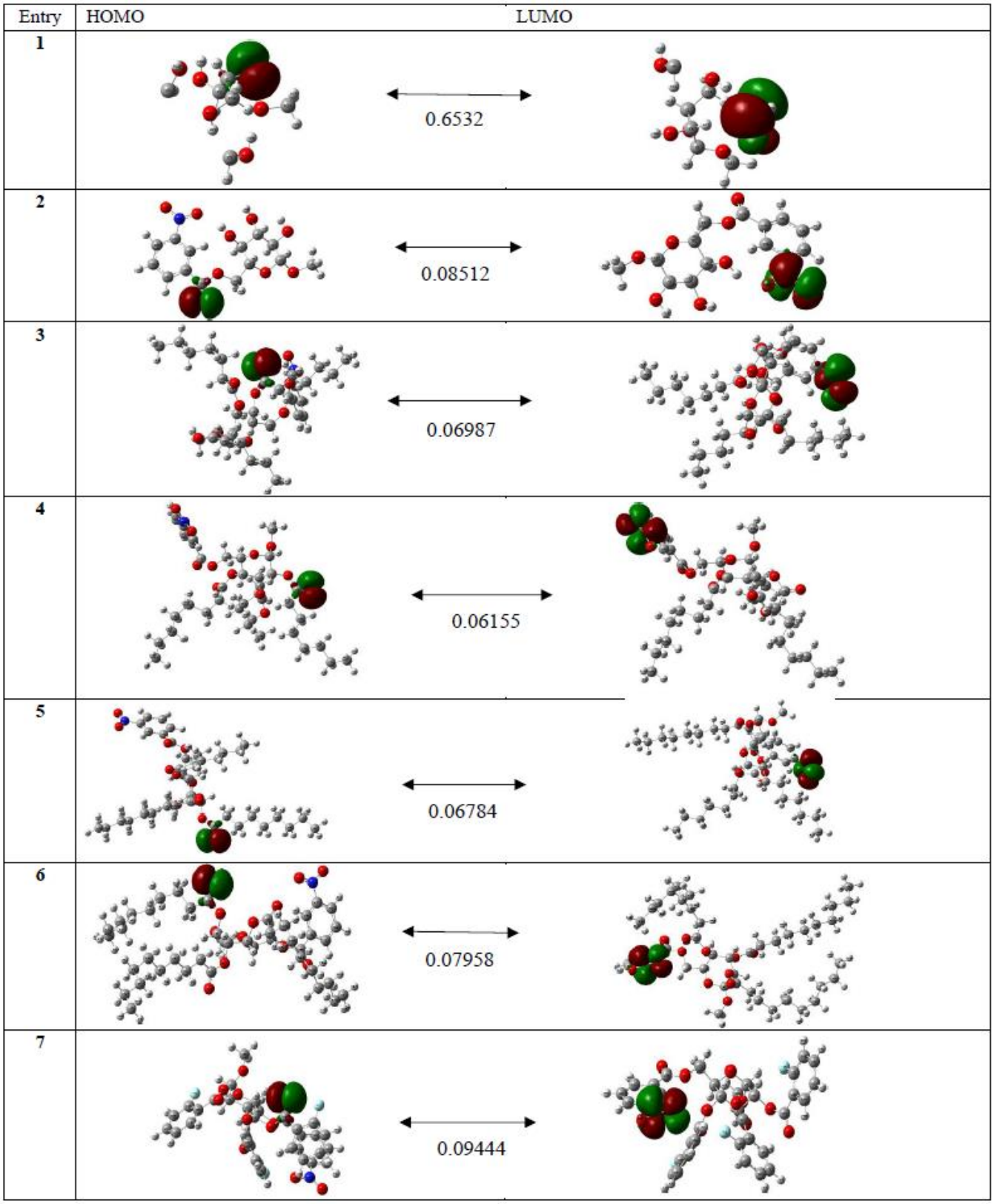

Fig. 3. Frontier molecular orbitals (HOMO and LUMO gaps) of Molecules **1-7**, which illustrate the distribution of the electron density. The HOMO is localized on the oxygen glycosidic moiety, and the LUMO is localized on the aromatic substituent.

Table 2. Thermodynamic Properties of MGP Derivatives (**1-7**)

Entry	Stoichiometry	Molecular weight (g mol^{-1})	Chemical potential (μ)	Enthalpy (Hartree)	Gibbs free energy (Hartree)	Dipole moment (Debye)
1	$C_7H_{14}O_6$	194.18	-0.14486	-717.8856	-717.9467	4.7309
2	$C_{14}H_{17}NO_9$	343.29	-0.22029	-1267.9731	-1268.0490	2.2652
3	$C_{35}H_{53}NO_{12}$	679.79	-0.20961	-2309.3717	-2309.5235	9.1153
4	$C_{38}H_{59}NO_{12}$	721.87	-0.21232	-2426.5894	-2426.7487	6.6078
5	$C_{41}H_{65}NO_{12}$	763.95	-0.20998	-2543.8009	-2543.9718	9.8334
6	$C_{44}H_{71}NO_{12}$	806.03	-0.19858	-2660.9992	-2661.1777	6.1873
7	$C_{35}H_{26}F_3NO_{12}$	709.58	-0.20484	-2591.3328	-2591.4591	3.6405

This suggested enhanced stability and reactivity across the derivatives. This trend aligns with the observed improvements in free energy and enthalpy values, reinforcing the role of structural modifications in optimizing molecular properties. The dipole moment plays a key role in drug design by influencing hydrogen bonding and nonbonded interactions, where a higher dipole moment can improve a molecule's binding affinity. Compound **5** had the highest dipole moment (9.833413 Debye), indicating strong polarity, whereas compound **2** presented the lowest dipole moment (2.265221 Debye). Additionally, some minor structural modifications might be used to enhance the thermal and molecular orbital properties. These findings highlight the importance of computational analysis in optimizing molecular stability and reactivity.

Molecular Electrostatic Potential (MEP)

A molecular electrostatic potential (MEP) map was employed to visualize the charge distribution and anticipate the reactive sites in the optimized structure of the MGP derivatives. It elucidates regions of electron richness (negative potential) and electron deficiency (positive potential), which are essential for comprehending chemical reactivity, intermolecular interactions, and solvent effects. This map also hints at significant charge separation in the molecule [44]. The MEP employs blue and red colors to depict sections of the molecule that are potentially vulnerable to electrophilic and nucleophilic assaults, respectively, whereas the green colors indicate zero potential regions. Hydrogen atoms have a high positive potential, whereas oxygen atoms have a strong negative potential. These different colors on the electrostatic potential map represent varying values of electrostatic potential across the molecule.

The red/orange/yellow regions observed around the oxygen atoms clearly indicate a high electron density area or negative potential (electron-rich, nucleophilic attack sites). On the other hand, the blue regions indicate the low-density area or positive potential (electron-deficient, electrophilic attack sites). The green color indicates the neutral regions. Therefore, nucleophilic reactions occur where the MEP is most positive (blue), and nucleophilic reactions occur where the MEP is most negative (red). The negative potential near lone pairs helps to predict hydrogen bonding [45]. The polarity and significant dipole moment of a compound align with its high hyperpolarizability, highlighted by the sharp contrast between these regions. Strong intermolecular interactions and superior docking performance can be obtained *via* polarization

By analyzing the electrostatic potential, we can determine the reactive sites and evaluate the polarity and charge distribution. A polar molecule is suggested by the asymmetrical distribution of electrostatic potential with a significant dipole moment. Symmetrical maps often indicate nonpolar molecules. The MEP maps in Fig. 4 for the parent compound, methyl α-D-glucopyranoside, and its derivatives visually forecast how the electrostatic potential is distributed over the surface of the molecule. Compound **3** had the lowest (most negative) potential (-6.182e-2), indicating that compound **3** became the most electron-rich and the most favorable candidate for electrophilic attack. Compounds with less negative MEP values may exhibit reduced reactivity toward electrophiles. The observed differences in potential distributions can be attributed to the number of acyl groups and aromatic moieties present in each molecule, which influence their overall charge distribution.

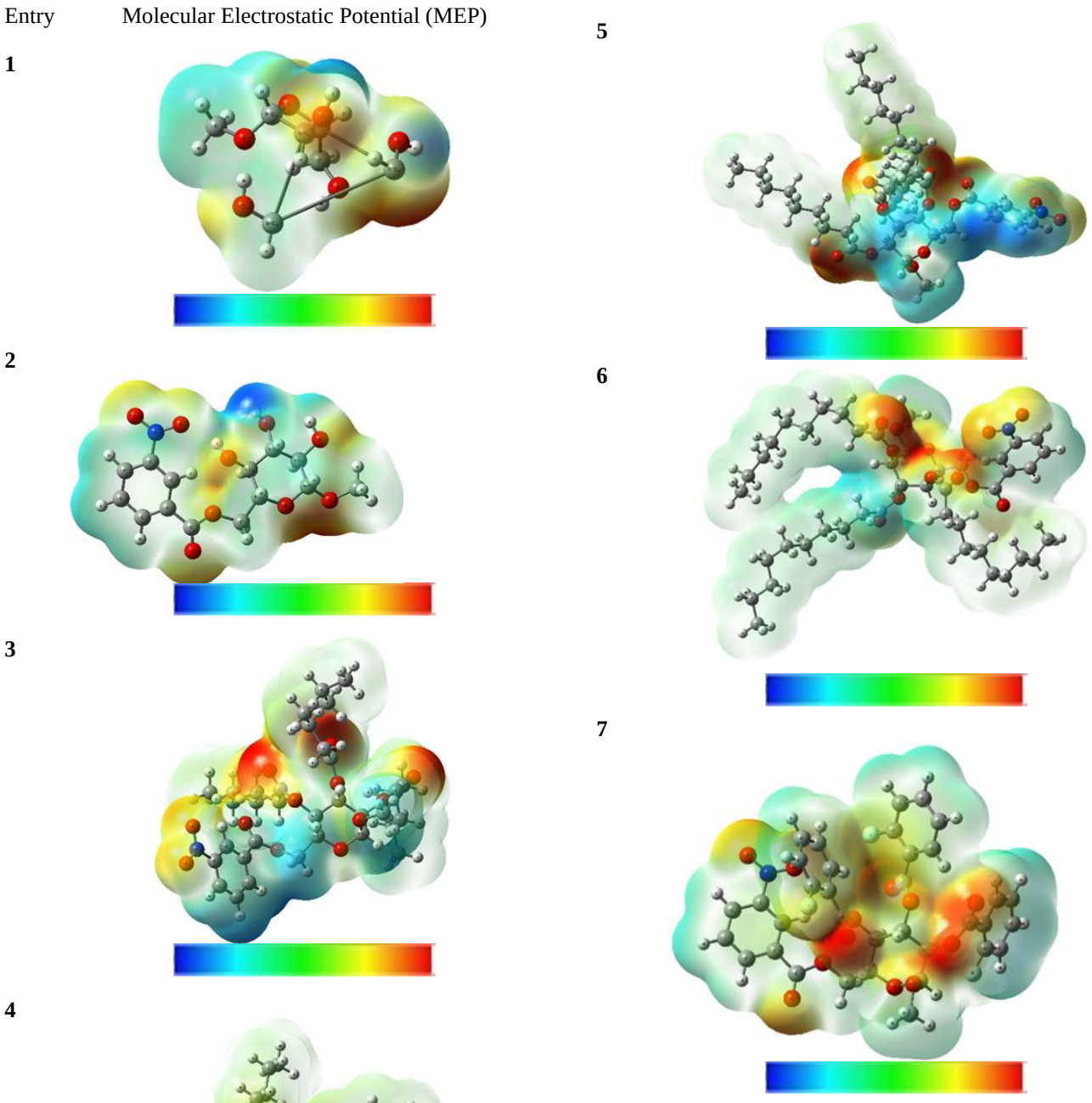

Fig. 4. Molecular electrostatic potential map of molecules (**1-7**). The red regions indicate electron-rich sites favorable for hydrogen bonding, whereas the blue regions are electron-deficient, highlighting potential interaction points with protein active sites.

Drug-Likeness Properties

To determine how these compounds are likely good oral drug candidates, we interpreted several parameters on the basis of their physicochemical properties and rule-based filters. The SwissADME provides the following rule-based filters: Lipinski's rule of five [46], the ghost filter, the Veber rule, the Egan rule, *etc*. Table 3 shows that each of the compounds has specific values for the parameters. The MR or molar refractivity here reflects the size and polarizability of a molecule. A value between 4 and 130 is ideal for drug-like behavior. We can also see that compounds **1** and **2** have lower iLOGP values than all the other compounds do, which indicates that they are less lipophilic and more hydrophilic. Compounds **3, 4, 5,** and **6** had values greater than **5**. Therefore, these compounds may have poor solubility and high toxicity. The value of compound **2** was within the ideal range; thus, it has good oral bioavailability, membrane permeability, and solubility. There was a distinct relationship between the structural alteration of the glucopyranoside derivatives and their ADMET behavior. Molecules **3-7**, which have bulky aromatic or acyl substituents, are significantly more lipophilic (iLOGP 4.3-8.38) and highly refractive (>160). These structural expansions substantially increase the hydrophobic surface area and steric bulk, which subsequently decreases gastrointestinal (GI) absorption as a result of low aqueous solubility and low membrane permeability.In contrast, molecules **1** and **2**, which have smaller and less hydrophobic substituents, exhibit lower iLOGP values (0.80-1.52), medium molecular refractivity, and molecular weights within the acceptable range. These structural characteristics help to increase the balance of polarity and provide better predicted absorption, which is reflected in the increased bioavailability scores (0.55). These findings reveal that a higher lipophilicity, aromatic concentration, and bulk of substituents have a catastrophic effect on the ADMET properties, whereas the accelerated polarity and smaller functional groups contribute to the enhanced ADMET behavior.

GI absorption is a qualitative prediction of whether a compound is likely to be well absorbed in the human gastrointestinal tract when taken orally. Generally, when the GI absorption value is high, the compound is predicted to be a good oral drug. However, these compounds have low GI values, which may indicate that some changes could lead to good oral drugs. BBB permeability refers to whether a compound can cross the blood-brain barrier [47,48]. Here, this prediction reveals the compounds that reach the central nervous system when taken orally. Owing to their permeability to the BBB, these compounds are unlikely to enter the brain. The bioavailability score of 0.55 suggests that the parent compound and compound **2** may be more promising for oral drugs. These compounds satisfy structural features and have a greater chance of being orally bioavailable in humans. Compounds **3**, **4**, **5**, and **6** are likely to have poor absorption or high metabolism. The drug-likeness score indicates how likely a compound is to become an oral drug on the basis of its physicochemical properties [49,50]. This score is mainly based on rule-based filters, such as Lipinski, Ghose, and Egan, and the bioavailability score. A negative or low score indicates that the compounds might have too many hydrogen bond donors, high molecular weights, or unfavorable logP values. Thus, the parent compound methyl α-D-glucopyranoside (**1**) might have favorable chemical structures for drug development and is likely to be well absorbed in the human body. Additionally, it can be predicted that compound **1** exhibits balanced solubility and permeability and does not possess excessive numbers of H-bond donors/acceptors.

Table 3. Pharmacokinetic Properties of MGP Derivatives

Molecule entry	MW	MR	iLOGP	GI absorption	BBB permeant	Bioavailability score	Drug-likeness model score
1	194.18	40.47	0.8	Low	No	0.55	0.12
2	343.29	78.93	1.52	Low	No	0.55	-0.41
3	679.79	180.24	5.14	Low	No	0.17	-0.66
4	721.87	194.66	6.56	Low	No	0.17	-0.74
5	763.95	209.09	7.11	Low	No	0.17	-0.74
6	806.03	223.51	8.38	Low	No	0.17	-0.74
7	709.58	167.72	4.3	Low	No	0.17	-0.40

Comparative Lipinski analysis revealed significant variations in the drug-likeness profiles of the seven glucopyranoside derivatives. Both molecules **1** and **2** meet all the significant Lipinski requirements, where the molecular weight of the molecule is less than 500 Da, the molecule is moderately lipophilic (iLOGP < 2), and the molecule has a reasonable bioavailability index (0.55). Their relatively small size and balanced polarity enhance their drug-likeness and improve their prospects for oral absorption.

Compounds **3-7**, on the other hand, do not pass the Lipinski rule because they break several parameters at the same time. The molecular weights (679-806 Da), iLOGP values (4.3-8.38), and molecular refractivities (>160) of these compounds are excessively high, suggesting a high degree of steric bulk and hydrophobicity. These properties result in low solubility, low permeability, and low-anticipated bioavailability (0.17). These violations accumulated, which is the reason why they had low drug-like model scores and poor oral activity. Drug-likeness models of the parent compound and MGP derivatives **2**, **3**, **5**, and **7**, which were investigated *via* MolSoft software, are displayed in Fig. 5. The drug-likeness score was calculated by analyzing properties such as molecular weight, lipophilicity (logP), hydrogen bond donors and acceptors, and rotatable bonds, following principles similar to Lipinski's rule of five. From the models, we can predict that compound **1** has the highest score and is considered more likely to exhibit favorable pharmacokinetic and pharmacodynamic profiles [51,52]. Structural modification, analog screening, and formulation strategies are needed for a low drug-likeness score, suggesting that their low bioavailability, poor absorption, or high toxicity risk are improved [53]. These data prioritize compounds with optimal scores, and researchers can streamline the drug discovery process and reduce the risk of late-stage failure.

Molecular Docking Exploration

To predict the interaction between a small molecule and a target protein, a computational technique known as molecular docking is used. It is a structure-based drug design method that helps in understanding how a drug binds to its receptor site at the molecular level [54]. Molecular docking was performed for compounds **1**, **2**, **3**, **4**, **5**, **6**, and **7** to investigate their binding mode.

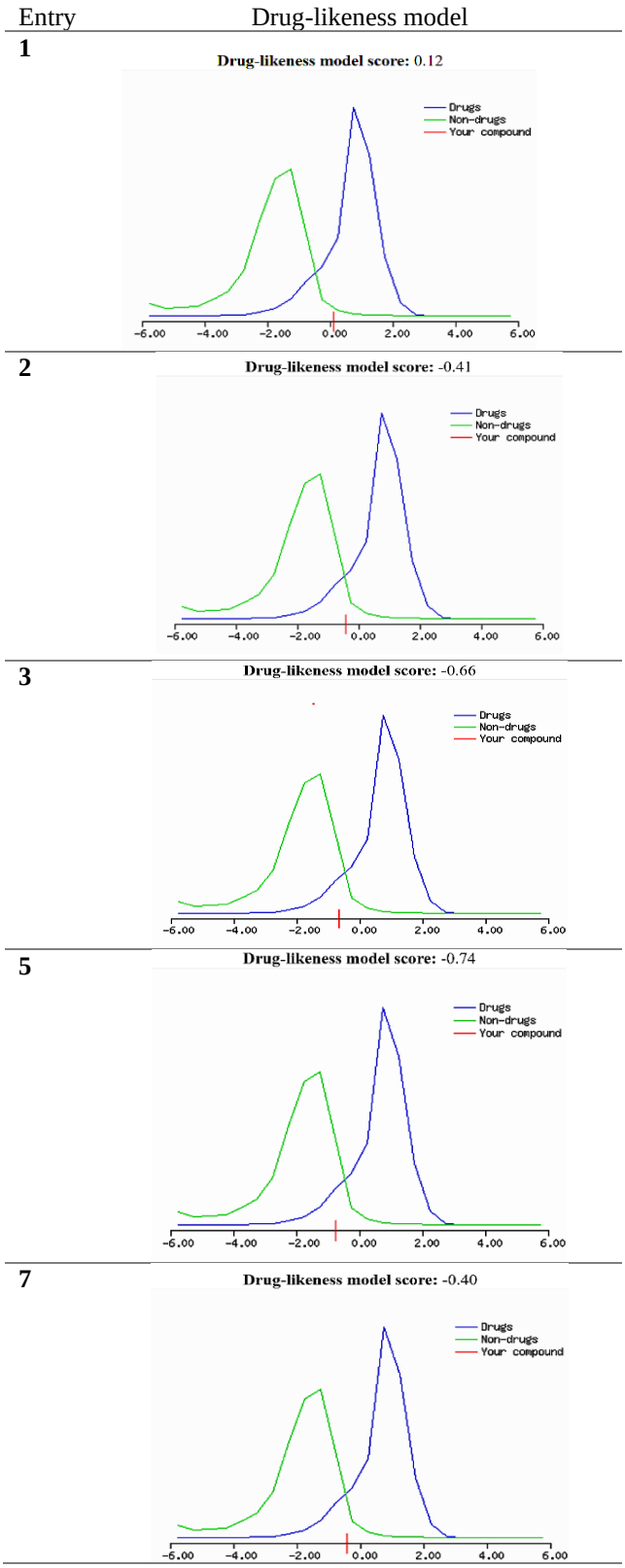

Fig. 5. Drug-likeness scores of MGP derivatives **2**, **3**, **5** and **7** generated *via* MOLSOFT.

All the designated derivatives were subjected to the same optimized docking conditions and docked into the same binding pocket (PDB ID: 4QWO). The binding affinity indicates how strongly a ligand (like a drug molecule) binds to a target protein or receptor [55,56]. The results of the docking analysis revealed that all the compounds had binding affinities ranging from -5.5 to -8.8 kcal mol^{-1}. Compared with the other derivatives, the parent compound had greater binding affinity. More negative values indicate stronger and more favorable binding, which can lead to the identification of the most promising drug candidates [57,58].

The docked conformation showed that the parent compounds and all the derivatives bind within the active site of the monkeypox virus (PDB ID: 4QWO) macromolecule structure. Table 4 shows that compounds **1** and **2** firmly bind through conventional hydrogen bonds with the residues ARG127, ARG119, ASP10, ASP123, ASN78, THR120, and GLU77. A closer distance was observed for GLU77. Compound **3** also presented a conventional hydrogen bond along with one pi-anion interaction with residue ASP127. Other derivatives, compounds **4** and **5**, which have binding affinities of -6.1 kcal mol^{-1} and -6.7 kcal mol^{-1}, respectively, exhibited hydrogen bonding interactions with residues such as HIS100, ARG127, ARG119, ARG129, ASN14, LYS16, etc. Hydrophobic alkyl bonding interactions were also observed between these two derivatives. ALA130 was the shortest distance from compound **5** in terms of alkyl bond interactions. Carbon-hydrogen bond interactions were also observed for compound **5** with residues ASP123 and HIS124. The binding affinity and the number of noncovalent interactions that occur in the binding pocket clearly correlate. The compounds with greater numbers of hydrogen bonds, especially to important residues such as ARG127, ARG119, and ASN78, presented greater binding affinities. An example of such a case is compound 7, which exhibited the best affinity (-8.6 kcal mol^{-1}) and contained several hydrogen bonds and halogen interactions; thus, it was strongly electrostatically stabilized. Similarly, compound 2 (-7.7 kcal mol^{-1}) also had five hydrogen bonds, which confirmed the same trend.

Conversely, compounds that had fewer hydrogen bonds (*e.g.*, 1, -5.5 kcal mol^{-1}) or compounds with hydrophobic contacts (*e.g.*, 4) had weaker binding. This association implies that hydrogen bonding is a dominant force in binding stability, whereas Pi-alkyl and alkyl interactions support total affinity.

Table 4 shows that compound **6** has a binding affinity of -6.0 kcal mol^{-1} and six similar binding sites, similar to previous compounds with ARG119, ARG127, ARG129, and HIS124. It also presented two new pi-alkyl bonds with residues TYR80 AND LYS60. These compounds interact firmly with the residue ARG127 at a shorter distance (1.96355 Å). Finally, compound **7** was observed to have the highest binding affinity, -8.6 kcal mol^{-1}. It forms a conventional hydrogen bond with the residues THR120 and ARG127, whereas an H-halogen interaction is shown by the residues HIS100 and ASN78. This derivative showed electrostatic pi-anion interactions with ASP123; pi-sigma interactions with ALA130; and pi-alkyl interactions with ARG119, LYS6, and ILE7 (shorter distance of 5.06891 Å). Table 4 shows that compounds bind with residues via conventional hydrogen bond interactions, pi-anion interactions, pi-alkyl interactions, pi-cation interactions, carbon-hydrogen interactions, and hydrogen–halogen interactions. Compound **5** showed the maximum hydrogen bonding interaction with residues, which led to an increase in the polarity of this compound.

Binding affinity analysis revealed that compound **7** had the highest binding affinity (-8.6 kcal mol^{-1}) for the active site residues, indicating that it had the most stable interaction. Interestingly, the ARG127, ARG119, HIS100, ASN78, and ASP123 residues are commonly represented in various complexes, indicating that the binding pocket is conserved. The binding stability of the compound was increased by the existence of several hydrogen bonds and halogen interactions (especially with fluorine in compound **7**), which was not the case with other ligands.

The affinities of compounds **2** and **5** were also relatively high (-7.7 and -6.7 kcal mol^{-1}, respectively), with a multitude of hydrogen bonds with ARG119, ARG127, and GLU77 as the main stabilizing forces. Conversely, the binding energies of compounds **1**, **3**, **4**, and **6** were relatively small (-5.5 to -6.5 kcal mol^{-1}), the number of H-bonds and length were lower, and hydrophobic or Pi-alkyl contacts were more common.

Table 4. Binding Affinity (kcal mol^{-1}) and Nonbonding Interactions of MGP Derivatives

Entry	Binding affinity (kcal mol^{-1})	Residue in contact	Interaction type	Distance
1	-5.5	ARG127	H-Bond	2.31761
		ASP10	H-Bond	2.71024
		ASP123	H-Bond	2.42963
		ASN78	H-Bond	2.64644
		THR120	Conventional H-Bond	3.56961
2	-7.7	ARG119	H-Bond	2.41784
		ARG119	H-Bond	2.20879
		ARG127	H-Bond	2.92727
		ARG127	H-Bond	2.31203
		GLU77	H-Bond	2.30976
3	-6.5	ARG129	H-Bond	2.20318
		ARG129	H-Bond	2.34855
		ARG127	H-Bond	1.93964
		HIS124	Conventional H-Bond	3.32166
		ASP127	Pi-Anion	3.86554
4	-6.1	HIS100	H-Bond	2.04684
		ARG129	H-Bond	2.20196
		ARG119	H-Bond	2.29391
		ARG119	H-Bond	2.43611
		ARG127	H-Bond	2.994
		ARG127	H-Bond	2.38611
		LYS6	Alkyl	4.58901
		ARG127	Alkyl	4.29449
		VAL128	Alkyl	4.4762
5	-6.7	ASN14	H-Bond	2.06452
		LYS16	H-Bond	2.02458
		ARG127	H-Bond	2.92831
		ARG127	H-Bond	1.84966
		ASN78	H-Bond	2.45179
		HIS124	Conventional H-Bond	3.47778
		ASP123	Conventional H-Bond	3.54504
		LYS6	Alkyl	4.25253
		ARG127	Alkyl	5.13588
		ALA130	Alkyl	3.90983
		LYS13	Alkyl	4.31714
6	-6	ARG129	H-Bond	2.13076
		HIS124	H-Bond	3.01669
		ARG127	H-Bond	1.96355
		HIS124	Conventional H-Bond	3.28346
		LYS6	Alkyl	3.95105
		ARG119	Alkyl	4.35661
		TYR80	Pi-Alkyl	4.95908
		LYS6	Pi-Alkyl	4.78896
7	-8.6	HIS100	H-Bond; Halogen (F)	2.38452
		THR120	H-Bond	2.50244
		ARG127	H-Bond	2.65949
		ASN78	Conventional H-Bond; Halogen (F)	3.13192
		ASP10	Conventional H-Bond	3.70363
		GLU77	Halogen (F)	3.05025
		ASN78	Halogen (F)	3.30404
		ASN78	Halogen (F)	3.47953
		ARG129	Halogen (F)	3.25015
		ASP123	Pi-Anion	3.39334
		ALA130	Pi-Sigma	3.56873
		ARG119	Pi-Alkyl	5.42831
		LYS6	Pi-Alkyl	5.06891
		ILE7	Pi-Alkyl	5.48144

Nonbonding interactions encompass hydrogen bonds, hydrophobic effects, ionic interactions, and π–π stacking, which collectively influence the binding affinity and selectivity between proteins and ligands. Recent studies have suggested that unconventional noncovalent interactions (NCIs), such as halogen bonds, sulfur–π interactions, and cation–π interactions, contribute to the fine-tuning of ligand binding and receptor activation. The geometrical characteristics and energetic landscape of noncovalent interactions at the binding interface of protein receptors and small ligands are obtained by specific noncovalent interactions at the protein–ligand interface. Various noncovalent interactions play significant roles and are often overlooked, but are important in the stabilization of protein–ligand complexes [59,60]. The nonbonding interactions of the parent compound and its derivatives are represented in Fig. 6.

The docked conformations and hydrogen bond surfaces of 4QWO with compounds **1**, **2**, **3, 4**, **5, 6**, and **7** are shown in Fig. 7. Docking analysis helps to predict the effectiveness of any compound as a drug by increasing the binding affinity of the resulting string. In drug design, it is important to understand where and how a molecule fits into the active sites [61]. This finding also highlights which parts of a molecule are most difficult to bind, indicating that more chemical modifications are needed to improve the potency of that compound. Spatial regions on a protein or ligand where hydrogen bonding interactions are most likely to occur, represented by hydrogen bond surfaces. These surfaces are critical in protein–ligand recognition, as hydrogen bonds contribute significantly to the binding orientation of the ligand within the active site. The identification of donor and acceptor groups, the optimization of ligand design, and the prediction of how structural modifications may alter binding affinity are facilitated by the visualization of hydrogen bond surfaces [62].

CONCLUSIONS

In this study, MGP derivatives were computationally studied to determine their potential biological activity. In these molecules, several investigations have been performed to identify properties such as biological activity, chemical reactivity, and frontier orbital studies such as the HOMO and LUMO. Additionally, favorable electrostatic regions contributing to ligand-protein interactions were identified *via* MEP analysis. The DFT results revealed distinct differences in the electronic behavior of the derivatives, where Molecule 1 and Molecule 2 had the most desirable HOMO–LUMO gaps and greater chemical softness, implying increased reactivity and greater potential to engage in charge transfer interactions. MEP analysis also revealed that the electronegative regions around the glycosidic oxygen sites were the main contributors to hydrogen bonding with the viral proteins. Molecular docking with the Monkeypox virus target protein identified Molecule 2 as the strongest binder and exhibited stable hydrogen-bond interactions with the essential active-site residues, preceded by the parent compound. Conversely, the docking affinities of the derivatives with large or highly hydrophobic substituents were weaker. ADMET analysis predictions indicated good oral bioavailability and low toxicity for some compounds. These analyses suggested that some modified versions of the parent compound might be more reactive. Overall, the quantum-chemical factors, electrostatic characteristics, docking factors, and pharmacokinetic characteristics suggest that molecule **2** is the most promising lead scaffold for use as a Monkeypox virus inhibitor, but the parent compound is still a promising lead scaffold. These preemptive observations provide a solid basis for future synthetic optimization and experimental validation of antiviral agents made of glucopyranosides.

ACKNOWLEDGMENTS

We gratefully acknowledge financial support from the Ministry of Science and Technology (MoST), Bangladesh (*Ref*.: SRG-246485, 05/03/2025).

Entry	Nonbonding interactions	Entry	Nonbonding interactions
1	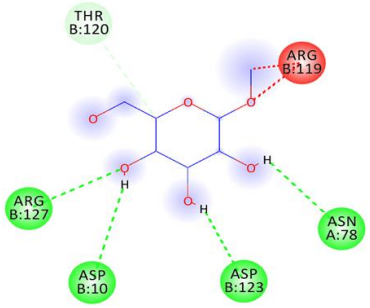	**2**	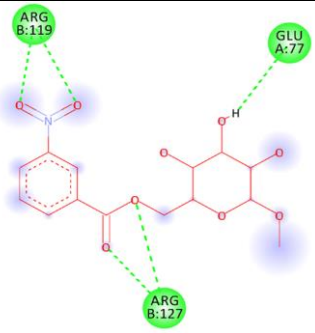
3	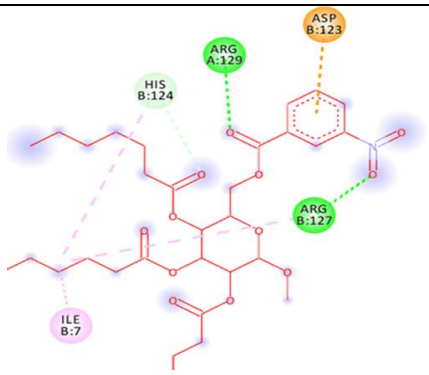	**4**	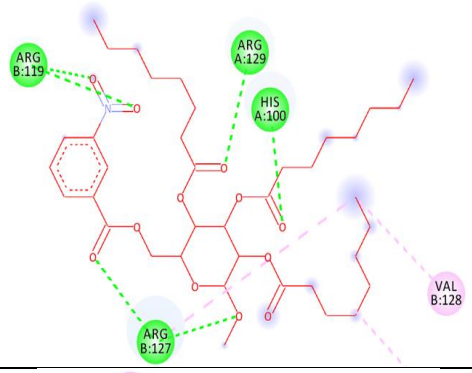
5	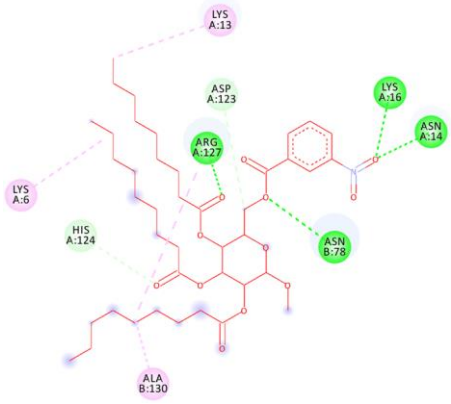	**6**	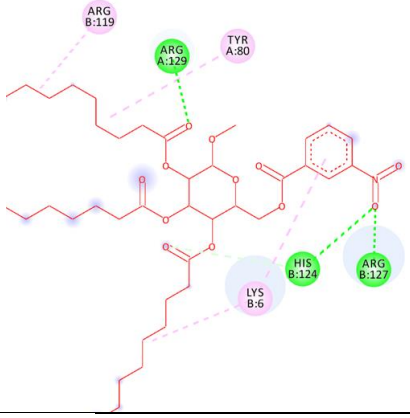
7	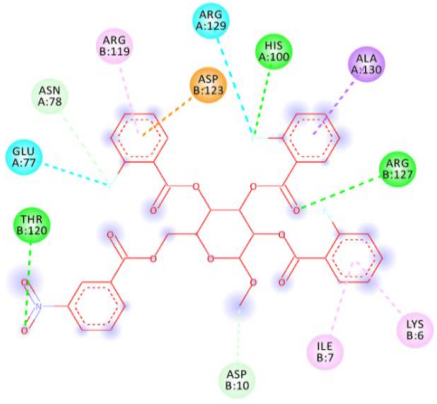		

Fig. 6. Nonbonding interactions of the parent compounds and MGP derivatives with the amino residues of 4QWO were performed *via* Discovery Studio.

Entry	Hydrogen bond surface	Active binding sites
1	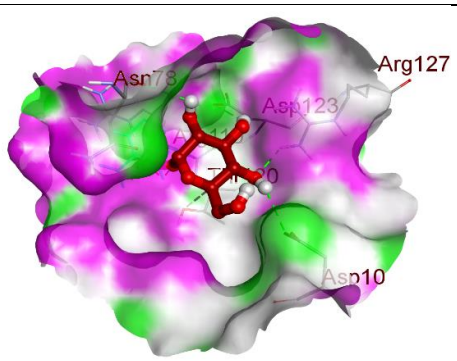	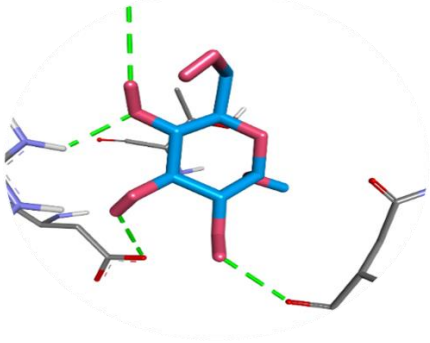
2	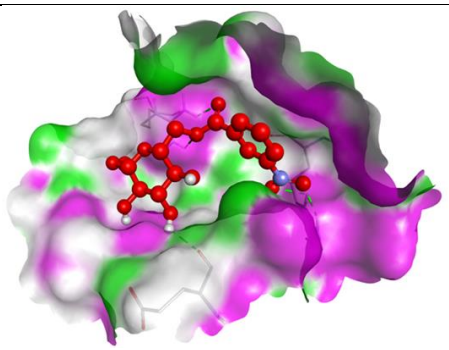	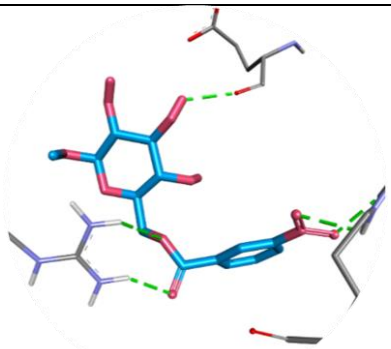
3	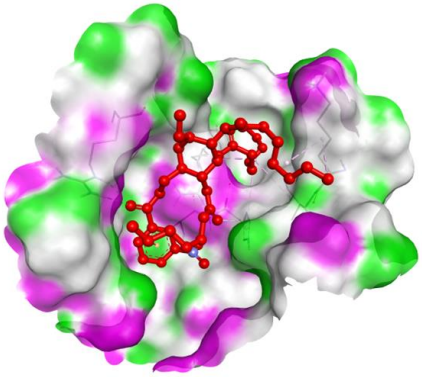	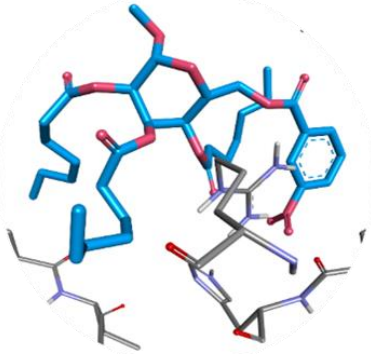
4	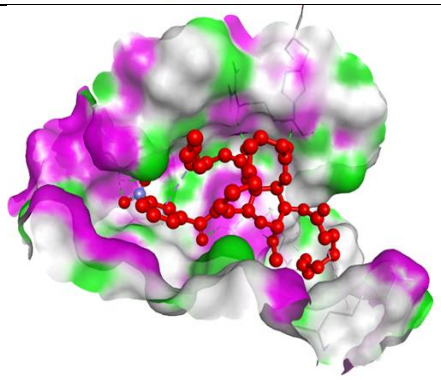	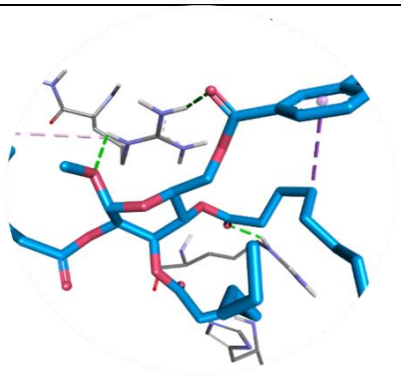

Fig. 7. The figure shows several important hydrogen bond interactions between the ligand and active site residues, suggesting that the derivatives are stably bound and inhibitory. The surface of compound **1** and MGP derivatives of the 4QWO inhibition binding site of the Monkeypox virus target protein, in hydrogen bonds, and the docked conformation.

5	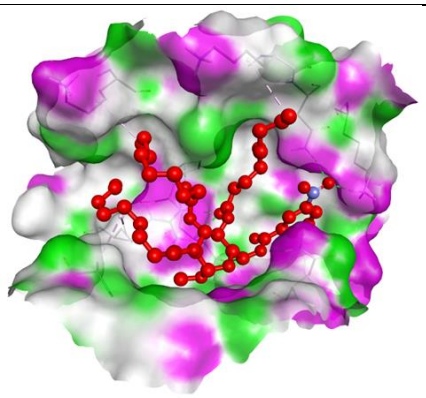	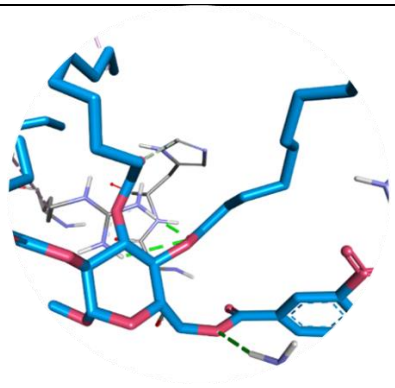
6	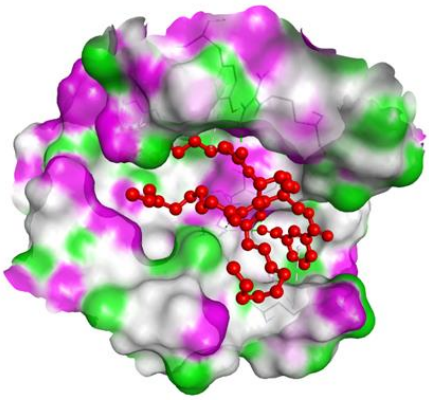	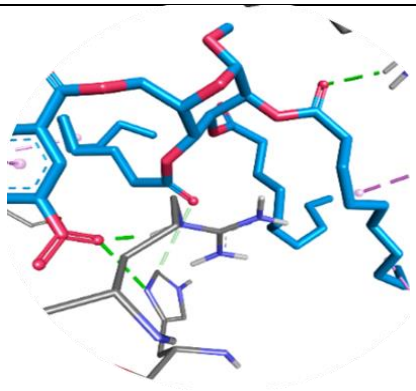
7	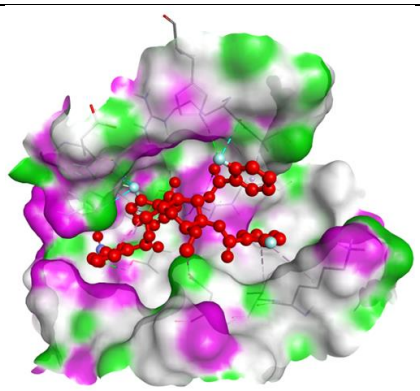	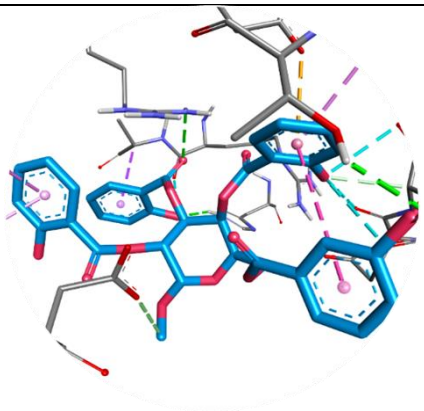

Fig. 7. Continued.

REFERENCES

[1] Cummings, J. H.; Stephen, A. M., Carbohydrate Terminology and Classification. *Eur. J. Clin. Nutr.* **2007**, *61* (S1) S5-S18. DOI: 10.1038/sj.ejcn.1602936.

[2] Khadka, Y. R., Carbohydrates-A Brief Deliberation with Bio-Aspect. *Cognition.* **2022,** *4* (1), 125-138. DOI: 10.3126/cognition.v4i1.46484.

[3] Li, J.; Ye, G.; Wang, J.; Gong, T.; Wang, J.; Zeng, D.; Cifuentes, A.; Ibañez, E.; Zhao, H.; Lu, W., Recent Advances in Pressurized Hot Water Extraction/Modification of Polysaccharides: Structure, Physicochemical Properties, Bioactivities, and Applications. *Compr Rev. Food Sci. Food Saf.* **2025**, *24* (1). DOI: 10.1111/1541-4337.70104.

[4] Deery, E.; Frank, S.; Lawrence, A.; Moore, S.; Schroeder, S.; Warren, M. J., Synthetic Biology in Metabolic Engineering: From Complex Biochemical Pathways to Compartmentalized Metabolic Processes - a Vitamin Connection. In *Encyclopedia Mol. Cell Biol. Mol. Med*. **2014**, 1-47. DOI: 10.1002/3527600906.mcb.20120075.

[5] Kawsar, S. M. A.; Matsumoto, R.; Fujii, Y.; Matsuoka, H.; Masuda, N.; Iwahara, C.; Yasumitsu, H.; Kanaly, R. A.; Sugawara, S.; Hosono, M.; Nitta, K.; Ishizaki, N.; Dogasaki, C.; Hamako, J.; Matsui, T.; Ozeki, Y., Cytotoxicity and glycan-binding profile of α-D-galactose-binding lectin from the eggs of a Japanese sea hare (*Aplysia kurodai*). *Protein J.* **2011**, *30* (7), 509-519. DOI: 10.1007/s10930-011-9356-7.

[6] Toukach, P. V.; Shirkovskaya, A. I., Carbohydrate Structure Database and Other Glycan Databases as an Important Element of Glycoinformatics. *Russ. J. Bioorg. Chem.* **2022**, *48* (3), 457-466. DOI: 10.1134/S1068162022030190.

[7] Kawsar, S. M. A.; Matsumoto, R.; Fujii, Y.; Yasumitsu, H.; Dogasaki, C.; Hosono, M.; Nitta, K.; Hamako, J.; Matsui, T.; Kojima, N.; Ozeki, Y., Purification and Biochemical Characterization of a D-Galactose Binding Lectin from Japanese Sea Hare (*Aplysia kurodai*) Eggs. *Biochem.* **2009**, *74* (7), 709-716. DOI: 10.1134/S0006297909070025.

[8] Akter, N.; Bourougaa, L.; Ouassaf, M.; Bhowmic, R. C.; Uddin, K. M.; Bhat, A. R.; Ahmed, S.; Kawsar, S. M. A., Molecular Docking, ADME-Tox, DFT and Molecular Dynamics Simulation of Butyroyl Glucopyranoside Derivatives against DNA Gyrase Inhibitors as Antimicrobial Agents. *J. Mol. Struct.* **2024**, *1307*, 137930. DOI: 10.1016/j.molstruc.2024.137930.

[9] Pan, L.; Cai, C.; Liu, C.; Liu, D.; Li, G.; Linhardt, R. J.; Yu, G., Recent Progress and Advanced Technology in Carbohydrate-Based Drug Development. *Curr. Opin. Biotechnol.* **2021**, *69*, 191–198. DOI: 10.1016/j.copbio.2020.12.023.

[10] Cao, X.; Du, X.; Jiao, H.; An, Q.; Chen, R.; Fang, P.; Wang, J.; Yu, B., Carbohydrate-Based Drugs Launched during 2000-2021. *Acta Pharm. Sinica B*. **2022**, 3783-3821. DOI: 10.1016/j.apsb.2022.05.020.

[11] Lagorce, D.; Douguet, D.; Miteva, M. A.; Villoutreix, B. O., Computational Analysis of Calculated Physicochemical and ADMET Properties of Protein-Protein Interaction Inhibitors. *Sci. Rep.* **2017**, *7* (1), 46277. DOI: 10.1038/srep46277.

[12] Arifuzzaman, M.; Islam, M. M.; Rahman, M. M.; Rahman, M. A.; Kawsar, S. M. A., An Efficient Approach to the Synthesis of Thymidine Derivatives Containing Various Acyl Groups: Characterization and Antibacterial Activities. *ACTA Pharm. Sci.* **2018**, *56* (4), 7-22. DOI: 10.23893/1307-2080.APS.05622.

[13] Kawsar, S. M. A.; Hamida, A. A.; Sheikh, A. U.; Hossain, M. K.; Shagir, A. C.; Sanaullah, A. F. M.; Manchur, M. A.; Imtiaj, H.; Ogawa, Y.; Fujii, Y.; Koide, Y.; Ozeki, Y., Chemically Modified Uridine Molecules Incorporating Acyl Residues to Enhance Antibacterial and Cytotoxic Activities. *Int. J. Org. Chem.* **2015**, *5* (4), 232-245. DOI: 10.4236/ijoc.2015.54023.

[14] Islam, M.; Arifuzzaman, A.; Rahman, M.; Rahman, M. A.; Kawsar, S. M. A., Novel Methyl 4,6-*O*-Benzylidene-α-D-Glucopyranoside Derivatives: Synthesis, Structural Characterization and Evaluation of Antibacterial Activities. *Hacett. J. Biol. Chem.* **2019**, *47* (2), 153-164. DOI: 10.15671/hjbc.622038.

[15] Kabir, A. K. M. S.; Kawsar, S. M. A.; Bhuiyan, M. M. R.; Rahman, M. S.; Chowdhury, M. E., Antimicrobial screening studies of some derivatives of methyl α-D-glucopyranoside. *Pak. J. Sci. Ind. Res.* **2009**, *52* (3), 138-142.

[16] Sklenovská, N.; Van Ranst, M., Emergence of Monkeypox as the Most Important Orthopoxvirus Infection in Humans. *Front. Public Health.* **2018**, *6*. DOI: 10.3389/fpubh.2018.00241.

[17] Tripathi, P.; Pandey, S.; Yadav, D.; Joshi, S., Emergence and Evolution of Monkeypox Virus: Epidemiology, Pathology, Clinical Symptoms, Preventative and Treatment Measures. *Int. Immunopharmacol.* **2025**, *152*, 114448. DOI: 10.1016/j.intimp.2025.114448.

[18] Waqas, M.; Shahid, S. A.; Shahab, M.; Zhu, Y.; Fahira, A.; Huang, Z., Structural and Computational Analysis of Monkeypox Virus Methyltransferase: Dynamic Inhibition Mechanisms and Their Implications for Antiviral Design. *Mol. Divers.* **2025**. DOI: 10.1007/s11030-025-11258-8.

[19] Gloriam, D. E., Bigger Is Better in Virtual Drug Screens. *Nature.* **2019**, *566* (7743), 193-194. DOI: 10.1038/d41586-019-00145-6.

[20] Dunkel, M., SuperNatural: A Searchable Database of Available Natural Compounds. *Nucleic Acids Res.* **2006**, *34* (90001), D678-D683. DOI: 10.1093/nar/gkj132.

[21] Begam, B. F.; Kumar, J. S., A Study on Cheminformatics and Its Applications on Modern Drug Discovery. *Proced. Eng.* **2012**, *38*, 1264-1275. DOI: 10.1016/j.proeng.2012.06.156.

[22] Jalbout, A. F.; Nazari, F.; Turker, L., Gaussian-Based Computations in Molecular Science. *J. Mol. Struct.* **2004**, *671* (1-3), 1-21. DOI: 10.1016/S0166-1280(03)00347-6.

[23] Danish Ahmad, A. V.; Khan, S. W.; Yasar, Q.; Shaikh, M. S.; Khan, M. M., Computational Biology Approach to Predict Molecular Mechanism in Cancer. *Oral Oncol. Rep.* **2024**, *12*, 100651. DOI: 10.1016/j.oor.2024.100651.

[24] Reveles, J. U.; Köster, A. M., Geometry Optimization in Density Functional Methods. *J. Comput. Chem.* **2004**, *25* (9), 1109-1116. DOI: 10.1002/jcc.20034.

[25] Zhuo, L.; Liao, W.; Yu, Z., A Frontier Molecular Orbital Theory Approach to Understanding the Mayr Equation and to Quantifying Nucleophilicity and Electrophilicity by Using HOMO and LUMO Energies. *Asian J. Org. Chem.* **2012**, *1* (4), 336-345. DOI: 10.1002/ajoc.201200103.

[26] Lima, L.; Barreiro, E., Bioisosterism: A Useful Strategy for Molecular Modification and Drug Design. *Curr. Med. Chem.* **2005**, *12* (1), 23-49. DOI: 10.2174/0929867053363540.

[27] Gleeson, M. P., Generation of a Set of Simple, Interpretable ADMET Rules of Thumb. *J. Med. Chem.* **2008**, *51* (4), 817-834. DOI: 10.1021/jm701122q.

[28] Pires, D. E. V.; Blundell, T. L.; Ascher, D. B., PkCSM: Predicting Small-Molecule Pharmacokinetic and Toxicity Properties Using Graph-Based Signatures. *J. Med. Chem.* **2015**, *58* (9), 4066-4072. DOI: 10.1021/acs.jmedchem.5b00104.

[29] Verma, V. V.; Vimal, S.; Mishra, M. K.; Sharma, V. K., A Comprehensive Review on Structural Insights through Molecular Visualization: Tools, Applications, and Limitations. *J. Mol. Model.* **2025**, *31* (6), 173. DOI: 10.1007/s00894-025-06402-y.

[30] Jagtap, M.; Girnar, G.; Ahuja, V., Computational Approaches to Molecular Docking and Protein Modeling in Drug Discovery. *J. Drug Deliv. Therapeut.* **2025**, *15* (6), 278-287. DOI: 10.22270/jddt.v15i6.7212.

[31] Śledź, P.; Caflisch, A., Protein Structure-Based Drug Design: From Docking to Molecular Dynamics. *Curr. Opin. Struct. Biol.* **2018**, *48*, 93-102. DOI: 10.1016/j.sbi.2017.10.010.

[32] Sert, Y., Pharmacokinetic Evaluation of Sulfadicramide through SwissADME: A Computational Insight into Drug-Likeness and Bioavailability. *MAS JAPS.* **2025**, *10* (2), 357-362. DOI: doi.org/10.5281/zenodo.15741944.

[33] Guan, L.; Yang, H.; Cai, Y.; Sun, L.; Di, P.; Li, W.; Liu, G.; Tang, Y., ADMET-Score – a Comprehensive Scoring Function for Evaluation of Chemical Drug-Likeness. *Medchemcomm.* **2019**, *10* (1), 148-157. DOI: 10.1039/C8MD00472B.

[34] Lee, K.; Jang, J.; Seo, S.; Lim, J.; Kim, W. Y., Drug-Likeness Scoring Based on Unsupervised Learning. *Chem. Sci.* **2022**, *13* (2), 554-565. DOI: 10.1039/d1sc05248a.

[35] Lipinski, C. A.; Lombardo, F.; Dominy, B. W.; Feeney, P. J., Experimental and Computational Approaches to Estimate Solubility and Permeability in Drug Discovery and Development Settings. *Adv. Drug Deliv. Rev.* **2012**, *64*, 4-17. DOI: 10.1016/j.addr.2012.09.019.

[36] Hodgson, J., ADMET Turning Chemicals into Drugs. *Nat. Biotechnol.* **2001**, *19* (8), 722-726. DOI: 10.1038/90761.

[37] Zhang, C. -R.; Liu, Z. -J.; Chen, Y. -H.; Chen, H. -S.; Wu, Y. -Z.; Feng, W.; Wang, D. -B., DFT and TD-DFT Study on Structure and Properties of Organic Dye Sensitizer TA-St-CA. *Curr. Appl. Phys.* **2010**, *10* (1), 77-83. DOI: 10.1016/j.cap.2009.04.018.

[38] Anowar H.; Alam, A.; Islam, M.; Fujii, Y.; Ozeki, Y.; Abe Kawsar, S. M., Geometrical Optimization, PASS Prediction, Molecular Docking, and in Silico ADMET Studies of Thymidine Derivatives against FimH Adhesin of Escherichia Coli. *Bulg. Chem. Commun.* **2021**, *53* (3), 327-342. DOI: 10.34049/bcc.53.3.5375.

[39] Nomura, Y.; Akashi, R., Density Functional Theory. *Encyclop. Condensed Matter Phys*. **2024**, 867-878. DOI: 10.1016/B978-0-323-90800-9.00148-7.

[40] Muthu, S.; Renuga, S., Molecular Orbital Studies (Hardness, Chemical Potential, Electronegativity and Electrophilicity), Vibrational Spectroscopic Investigation and Normal Coordinate Analysis of 5-{1-Hydroxy-2-[(Propan-2-Yl)Amino]Ethyl}benzene-1,3-Diol. *Spectrochim. Acta A Mol. Biomol. Spectrosc.* **2014**, *118*, 683-694. DOI: 10.1016/j.saa.2013.09.035.

[41] Zhao, X.; Chen, C.; Sun, Q.; Li, Y.; Yu, H., Molecular Structure Optimization Design of Inhibitors Based on Frontier Orbitals Theory. *Appl. Surf. Sci.* **2019**, *494*, 895-907. DOI: 10.1016/j.apsusc.2019.07.248.

[42] Jiménez, J. S.; Benítez, M. J., Gibbs Free Energy and Enthalpy–Entropy Compensation in Protein-Ligand Interactions. *Biophysica.* **2024**, *4* (2), 298-309. DOI: 10.3390/biophysica4020021.

[43] Demirel, Y.; Gerbaud, V., Fundamentals of Equilibrium Thermodynamics. *Nonequilibrium Thermodynamics*; *Elsevier*. **2019**, 1-85. DOI: 10.1016/B978-0-444-64112-0.00001-0.

[44] Scrocco, E.; Tomasi, J., The Electrostatic Molecular Potential as a Tool for the Interpretation of Molecular Properties. *Springer*. **2007**, 95-170. DOI: 10.1007/3-540-06399-4_6.

[45] Politzer, P.; Murray, J. S., Computational Prediction of Condensed Phase Properties from Statistical Characterization of Molecular Surface Electrostatic Potentials. *Fluid Phase Equilib*. **2001**, *185* (1-2), 129-137. DOI: 10.1016/S0378-3812(01)00463-0.

[46] Nhlapho, S.; Nyathi, M.; Ngwenya, B.; Dube, T.; Telukdarie, A.; Munien, I.; Vermeulen, A.; Chude-Okonkwo, U., Druggability of Pharmaceutical Compounds Using Lipinski Rules with Machine Learning. *Sci. Pharm.* **2024**, *3* (4), 177-192. DOI: 10.58920/sciphar0304264.

[47] Zhao, Y.; Gan, L.; Ren, L.; Lin, Y.; Ma, C.; Lin, X., Factors Influencing the Blood-Brain Barrier Permeability. *Brain Res.* **2022**, *1788*, 147937. DOI: 10.1016/j.brainres.2022.147937.

[48] Chalkha, M.; Chebbac, K.; Nour, H.; Nakkabi, A.; El Moussaoui, A.; Tüzün, B.; Bourhia, M.; Chtita, S.; Bakhouch, M.; Laaroussi, H.; Kawsar, S. M. A., Hadda, T. B.; Houari, G. A.; Maria, A.; Aboul-Soud, M. A. M.; El Yazidi. M., *In vitro* and *in silico* evaluation of the antimicrobial and antioxidant activities of spiropyrazoline oxindole congeners. *Arab. J. Chem.* **2024**, *17* (1), 105465. DOI: 10.1016/j.arabjc.2023.105465.

[49] Ursu, O.; Rayan, A.; Goldblum, A.; Oprea, T. I., Understanding Drug-likeness. *WIREs Comput. Mol. Sci.* **2011**, *1* (5), 760-781. DOI: 10.1002/wcms.52.

[50] Munia, N. S.; Hosen, M. A.; Azzam, K. M. A.; Al-Ghorbani, M.; Baashen, M.; Hossain, M. K.; Ali, F.; Mahmud, S.; Shimu, Mst. S. S.; Almalki, F. A.; Hadda, T. B.; Laaroussi, H.; Naimi, S.; Kawsar, S. M. A., Synthesis, Antimicrobial, SAR, PASS, Molecular Docking, Molecular Dynamics and Pharmacokinetics Studies of 5′- *O* -Uridine Derivatives Bearing Acyl Moieties: POM Study and Identification of the Pharmacophore Sites. *Nucleos. Nucleot. Nucl. Acids.* **2022**, *41* (10), 1036-1083. DOI: 10.1080/15257770.2022.2096898.

[51] Sampat, G.; Suryawanshi, S. S.; Palled, M. S.; Patil, A. S.; Khanal, P.; Salokhe, A. S., Drug Likeness Screening and Evaluation of Physicochemical Properties of Selected Medicinal Agents by Computer Aided Drug Design Tools. *Adv. Pharmacol. Pharm.* **2022**, *10* (4), 234-246. DOI: 10.13189/app.2022.100402.

[52] Kawsar, S. M. A.; Huq, E.; Nahar, N., Cytotoxicity Assessment of the Aerial Parts of Macrotyloma

Uniflorum Linn. *Int. J. Pharmacol.* **2008**, *4* (4), 297-300. DOI: 10.3923/ijp.2008.297.300.

[53] Souza, A. S. de; Amorim, V. M. de F.; Soares, E. P.; de Souza, R. F.; Guzzo, C. R., Antagonistic Trends Between Binding Affinity and Drug-Likeness in SARS-CoV-2 Mpro Inhibitors Revealed by Machine Learning. *Viruses.* **2025**, *17* (7), 935. DOI: 10.3390/v17070935.

[54] Kawsar, S. M. A.; Munia, N. S.; Saha, S.; Ozeki, Y., *In Silico* Pharmacokinetics, Molecular Docking and Molecular Dynamics Simulation Studies of Nucleoside Analogs for Drug Discovery- A Mini Review. *Mini-Rev. Med. Chem.* **2024**, *24* (11), 1070-1088. DOI: 10.2174/0113895575258033231024073521.

[55] Yuriev, E.; Ramsland, P. A., Latest Developments in Molecular Docking: 2010-2011 in Review. *J. Mol. Recog.* **2013**, *26* (5), 215-239. DOI: 10.1002/jmr.2266.

[56] Lafridi, H.; Almalki, F. A.; Ben Hadda, T.; Berredjem, M.; Kawsar, S. M. A.; Alqahtani, A. M.; Esharkawy, E. R.; Lakhrissi, B.; Zgou, H., *In Silico* Evaluation of Molecular Interactions between Macrocyclic Inhibitors with the HCV NS3 Protease. Docking and Identification of Antiviral Pharmacophore Site. *J. Biomol. Struct. Dyn.* **2023**, *41* (6), 2260-2273. DOI: 10.1080/07391102.2022.2029571.

[57] Pantsar, T.; Poso, A., Binding Affinity via Docking: Fact and Fiction. *Molecules.* **2018**, *23* (8), 1899. DOI: 10.3390/molecules23081899.

[58] Gu, Y.; Zhang, X.; Xu, A.; Chen, W.; Liu, K.; Wu, L.; Mo, S.; Hu, Y.; Liu, M.; Luo, Q., Protein-Ligand Binding Affinity Prediction with Edge Awareness and Supervised Attention. *IScience.* **2023**, *26* (1), 105892. DOI: 10.1016/j.isci.2022.105892.

[59] Zhou, P.; Huang, J.; Tian, F., Specific Noncovalent Interactions at Protein-Ligand Interface: Implications for Rational Drug Design. *Curr. Med. Chem.* **2012**, *19* (2), 226-238. DOI: 10.2174/092986712803414150.

[60] Anighoro, A., Underappreciated Chemical Interactions in Protein-Ligand Complexes**.** *Meth. Mol. Biol. Quant. Mechan. Drug Discov.* **2020**, 75-86. DOI: 10.1007/978-1-0716-0282-9_5.

[61] Agu, P. C.; Afiukwa, C. A.; Orji, O. U.; Ezeh, E. M.; Ofoke, I. H.; Ogbu, C. O.; Ugwuja, E. I.; Aja, P. M., Molecular Docking as a Tool for the Discovery of Molecular Targets of Nutraceuticals in Diseases Management. *Sci. Rep.* **2023**, *13* (1). DOI: 10.1038/s41598-023-40160-2.

[62] Wagner, S. C.; Ichim, T. E.; Bogin, V.; Min, W.-P.; Silva, F.; Patel, A. N.; Kesari, S., Induction and Characterization of Anti-Tumor Endothelium Immunity Elicited by ValloVax Therapeutic Cancer Vaccine. *Oncotarget.* **2017**, *8* (17), 28595-28613. DOI: 10.18632/oncotarget.15563.